1   **Sound absorption of porous substrates covered by foliage: experimental results and**

2   **numerical predictions**

3

4   Lei Ding, Timothy Van Renterghem,[a] Dick Botteldooren,

5   Department of Information Technology, Ghent University, St.-Pietersnieuwstraat 41, 9000 Gent,

6   Belgium

7   Kirill Horoshenkov and Amir Khan

8   School of Engineering, University of Bradford, Bradford, BD7 1DP, UK.

9   (Dated: July 13, 2012)

[a] timothy.van.renterghem@intec.ugent.be

Abstract

The influence of loose plant leaves on the acoustic absorption of a porous substrate is experimentally and numerically studied. Such systems are typical in vegetative walls, where the substrate has strong acoustical absorbing properties. Both experiments in an impedance tube and theoretical predictions show that when a leaf is placed in front of such a porous substrate, its absorption characteristics markedly change (for normal incident sound). Typically, there is an unaffected change in the low frequency absorption coefficient (below 250 Hz), an increase in the middle frequency absorption coefficient (500 Hz - 2000 Hz) and a decrease in the absorption at higher frequencies. The influence of leaves becomes most pronounced when the substrate has a low mass density. A combination of the Biot's elastic frame porous model, viscous damping in the leaf boundary layers and plate vibration theory is implemented via a finite-difference time-domain model, which is able to predict accurately the absorption spectrum of a leaf above a porous substrate system. The change in the absorption spectrum caused by the leaf vibration can be modeled reasonably well assuming the leaf and porous substrate properties are uniform.

PACS numbers: 43.28.En, 43.40.Fz, 43.58.Bh

I. INTRODUCTION

This paper considers the specific case of a porous medium covered by a plant leaf. This situation is of interest to outdoor sound propagation studies whereby the presence of plant leaves can have an influence on the ground effect, on green roof absorption, and on the absorption coefficient of green walls.

Although the importance of the soil effect when considering acoustic noise reduction by vegetation belts is well recognized[1,2], there have not been any systematic studies on the effect of plant leaves. It is known that the presence of vegetation makes the ground more porous and thus acoustically softer. This process is caused by rooting of plants and by a layer of humus which results from plant litter. This specific type of soil is often referred to as a "forest floor". This is a dynamic process in which the presence of leaves cannot be ignored and the effect of a layer of leaves on the ground attenuation is yet to be theoretically explained.

Another case of interest is the absorption by a green wall. Such a system consists of a highly porous and light-weight soil substrate layer which is mechanically attached to a building facade. The substrate is used to grow small plants. These plants develop into foliage which covers densely the porous substrate and might affect its acoustic absorption properties. The substrates typically used for wall vegetation exhibit high values of the absorption coefficient[3,4] and can be adopted in noise abatement applications in an urban environment. These applications include cases where multiple reflections between parallel reflecting building facades lead to a strong amplification of the environmental noise level. It has been demonstrated that increasing wall

1   absorption in a city street generally results in a noticeable noise reduction in an adjacent city

2   canyon as well[5,6]. Acoustically efficient plants can also be planted in a porous substrate deposited

3   on a green roof to reduce the diffraction of acoustic noise into quiet areas[7]. Wall vegetation and

4   green roof systems can also be applied to classical noise barriers to reduce the effects of multiple

5   reflections and diffraction of noise into the shadow zone behind the barriers[3].

6   An important question which is addressed in this paper is whether the presence of plant

7   leaves can result in a noticeable change in the absorption coefficient of a porous layer which

8   represents the acoustic behavior of the soil substrate in a green wall or the behavior of a porous

9   forest floor covered with leaves. In this study, experiments in an impedance tube have been

10   performed to study the basic phenomenon of this interaction. A fully controlled measurement

11   setup such as the one which is reported in this work enables validation of the proposed numerical

12   approach. The numerical modeling approach adopted here is based on time-domain modeling.

13   A porous substrate can often be simulated by the rigid frame model, which assumes that only

14   the air inside the porous medium vibrates. Some examples can be found in the work by Van

15   Renterghem and Botteldooren[8,9], and Salomons et al.[10] It has been shown that the rigid frame

16   model can provide a reasonable parameter fit to model the reflection from typical outdoor soils[11].

17   However, there are situations where the frame density is relatively small so that the frame

18   vibrations cannot be neglected. In these situations the acoustic characteristics of the material

19   frame must be taken into account. This is the case for one of the low-density porous substrates

20   used in the experiments presented in this paper. In Ref.12, a discussion on the validity of the

21   Zwikker and Kosten model, a rigid frame model that is often applied in the FDTD context, can

be found. Since in the current study much higher frequencies are looked at, then in typical

(outdoor) noise control applications, the use of more advanced models might be needed[12].

Accurately modeling the substrate behavior is of importance in this study, since the interaction

between leaves and substrate is expected to be a secondary effect. Also for consistency, the same

model has been applied to both types of substrates considered in this study.

In this work, the Biot[13,14] model is used to predict the coupled movement of the elastic

frame and fluid inside the porous medium. The model is implemented as an extension of the

finite-difference time-domain approach.

The bending wave equation for a thin uniform and homogeneous plate[15] is used to model

the vibration of a loose leaf rested just above the porous substrate. Plate vibration damping and

viscous boundary layer absorption on the leaf surface are the main mechanisms for acoustic

energy loss.

This paper is organized in the following way. In Sec. II, the governing equations for sound

propagation through a poro-elastic substrate in combination with leaf vibrations are presented

together with the finite-difference time-domain technique which is used to solve these equations.

An impedance tube experiment that is used to validate the developed numerical method is

described in Sec. III. The absorption coefficients of the porous substrate with and without a leaf

are studied experimentally. In Sec. IV, the simulations are compared against the measured data.

In Sec. V, a parametric analysis is carried out to illustrate the influence of leaf surface density on

the absorption coefficient of the porous substrate covered by a leaf. The final conclusions are

drawn in Sec. VI.

1

II. THEORY AND METHOD

A. Theoretical model

The propagation of acoustic waves in homogeneous and non-moving air is governed by the

continuity equation and the momentum equation

$$\frac{\partial p}{\partial t} + \rho_0 c^2 \nabla \cdot \mathbf{V} = 0, \tag{1}$$

$$\rho_0 \frac{\partial \mathbf{V}}{\partial t} = -\nabla p, \tag{2}$$

where p is the acoustic pressure, c is the speed of sound, ρ_0 is the mass density of air,

$\mathbf{V} = (v_x, v_y, v_z)$, and v_x, v_y and v_z are the components of the particle velocity vector in x, y and

z directions, respectively.

The propagation of acoustic waves in porous elastic media can be formulated based on the

dynamic equations and stress-strain relation in Biot's theory[13, 14]. This leads to continuity and

momentum equations for both the fluid inside the frame (see Eqs. (3) and (4)), and the frame

itself (see Eqs. (5) and (6)):

$$-\frac{\partial p_a}{\partial t} = K_a v_a \nabla \cdot \mathbf{V}_a + (K_a - P_0) v_f \nabla \cdot \mathbf{V}_f, \tag{3}$$

$$\rho_a \frac{\partial \mathbf{V}_a}{\partial t} = -\nabla p_a - \sigma(\mathbf{V}_a - \mathbf{V}_f)$$

$$-\rho_a \left(\frac{m_t}{v_a^2} - 1 \right) \frac{\partial}{\partial t} (\mathbf{V}_a - \mathbf{V}_f), \tag{4}$$

$$-\frac{\partial p_f}{\partial t} + \frac{v_f}{v_a} \frac{\partial p_a}{\partial t} = K_f \nabla \cdot \mathbf{V}_f, \tag{5}$$

19

1 $$\rho_f \frac{\partial \mathbf{V}_f}{\partial t} + R_f \mathbf{V}_f = -\nabla p_f + \sigma\left(\mathbf{V}_a - \mathbf{V}_f\right)$$

2 $$+ \rho_a \left(\frac{m_t}{v_a^2} - 1\right)\frac{\partial}{\partial t}\left(\mathbf{V}_a - \mathbf{V}_f\right), \tag{6}$$

3 where ρ_a is the mass of fluid per unit bulk volume; K_a is the bulk modulus of the fluid; p_a

4 is the pressure of fluid in the porous medium; v_a is the porosity; $v_f = 1 - v_a$; P_0 is the

5 ambient atmospheric pressure; $\mathbf{V}_a = (v_{xa}, v_{ya}, v_{za})$, and v_{xa}, v_{ya} and v_{za} are the air-particle

6 velocity components in x, y and z directions inside the porous medium, respectively; p_f is the

7 pressure on the solid frame; $\mathbf{V}_f = (v_{xf}, v_{yf}, v_{zf})$, and v_{xf}, v_{yf} and v_{zf} are the frame velocity

8 components in x, y and z directions, respectively; m_t is the tortuosity; σ is the flow resistivity;

9 ρ_f is the density of the frame material; K_f is the bulk modulus of the solid frame; and R_f is

10 the coefficient for an extra damping term added to the momentum equation of solid frame in

11 order to approximate dissipation mechanisms other than those caused by the flow resistivity. This

12 term is different from that described in Biot's work[13, 14]. Biot suggested replacing flow velocity,

13 bulk elasticity, etc. by complex functions of frequency to account for non- or different damping

14 mechanisms in the solid fraction. In theory, these complex functions could be approximated by

15 digital filters and transformed to time domain, like will be done in Eq. (24) for viscous boundary

16 layers, but this complicates equations considerably while stability is not guaranteed. The first

17 order approximation obtained by introducing R_f induces the basic frame damping that is needed

18 to reproduce the measured results, at a lower computational cost. The parameters, such as K_a,

19 P_0, K_f, σ and m_t, can be related to the parameters in Biot's papers[13, 14].

20   The vibration of a leaf in the vicinity of a porous substrate is modeled using the theory of

1   vibrating thin plates[15]. The viscoelastic damping during the leaf vibration can be included by

2   employing the generalized Maxwell model, which has been used in the work of Chaigne et

3   al.[16,17] The leaf is approximated by an acoustically infinitely thin plate forming the shape of the

4   leaf. Bending waves can propagate in the two in-plane directions. Assuming that the plate is

5   orthogonal to x direction, the velocity equation can be written as

$$
6 \quad \rho_m h \left(\frac{\partial v_{xp}}{\partial t} + R_L v_{xp} \right)
$$

$$
7 \quad = -\frac{\partial p}{\partial x} h - \frac{\partial^2 \phi_0}{\partial y^2} - \frac{\partial^2 \phi_0}{\partial z^2} - \frac{\partial^2 \phi}{\partial y^2} - \frac{\partial^2 \phi}{\partial z^2} , \tag{7}
$$

8   where ρ_m is the surface mass density of the plate material (in kg/m^2); h is the thickness of the

9   plate; v_{xp} is the plate velocity vector component in the x direction; R_L denotes the viscous

10   damping in the bending process; and ϕ_0 denotes the bending and twisting moments per unit

11   thickness. Assuming that the leaf is isotropic, it can be formulated as

$$
12 \quad \phi_0 = D \frac{\partial^2 w}{\partial y^2} + D \frac{\partial^2 w}{\partial z^2} , \tag{8}
$$

13   where D is the bending stiffness per unit width for plate; w is the displacement component in x

14   direction and its time derivative is the velocity v_{xp}. ϕ in Eq. (7) denotes the viscoelastic

15   damping during the bending of leaf and the damping occurs at a distribution of times according

16   to generalized Maxwell model. It can be formulated as

$$
17 \quad \frac{\partial \phi}{\partial t} = \sum_{n=1}^{\infty} DR_n \Pi_n , \tag{9}
$$

$$
18 \quad \Pi_n = \frac{\partial^2 w}{\partial y^2} + \frac{\partial^2 w}{\partial z^2} - \int_0^t \left(\frac{\partial^2 w}{\partial y^2} + \frac{\partial^2 w}{\partial z^2} \right) e^{-s_n(t-\tau)} s_n d\tau , \tag{10}
$$

1 where R_n and s_n are the viscoelastic damping parameters, which can be determined by

2 data-fitting with measurement results. Equations (7) - (10) can be derived from Chaigne et al.'s

3 work[16,17] by using inverse Laplace transform and assuming that the plate is isotropic. In this

4 paper, the viscoelastic damping and the viscous damping parameters for leaves will be chosen

5 with reference to the data used in modeling the bending of wood (see Ref. 16), and they are

6 $R_1 = 0.013$, $R_2 = 0.038$, $s_1 = 2000 rad/s$, $s_2 = 33000 rad/s$ and $R_L = 2.4 s^{-1}$.

7 Close to the objects, viscosity (and thermal conductivity) cannot be ignored since viscous

8 energy decay in the boundary layer at the surface of the leaves is one of the mechanisms causing

9 sound attenuation[18]. As in Ref. 19, a time-domain approximation for a viscous boundary layer near

10 an infinitely extended flat surface will be used. The viscosity adds an additional term (in frequency

11 domain) to the linearized momentum equations (see Eq. (2)) in the directions which are parallel to

12 the leaf surface plane:

13 $$\frac{\Im k_n}{d_{BL}} \langle v_\gamma \rangle, \text{ with } k_n^2 = \Im \omega \frac{\rho_0}{\mu}, \tag{11}$$

14 where the subscript in v_γ denotes that the velocity is parallel to the leaf surface plane, $\langle \ \rangle$

15 denotes that the velocity v_γ is averaged over a layer thickness d_{BL}; μ is the dynamic

16 viscosity of air; ω is the angular frequency and $\Im = \sqrt{-1}$ is the imaginary unit.

17

18 **B. Finite-difference time-domain method**

19 The finite-difference time-domain method can be used to solve the set of equations

20 presented in Sec. IIA. In this paper, the staggered grid organization, both in space and time, as

9

1 suggested in Ref.[20] is considered. A leap-frog scheme is used to update acoustic pressure and

2 velocity components over time. Using this method, second-order accuracy can be obtained in

3 representing the spatial derivatives, with the smallest possible stencil. The spatial organization of

4 some cells near the interface between the porous substrate and air, including a leaf, are illustrated

5 in Fig. 1. For this specific scheme, the following notations are commonly used to represent the

6 discrete pressures and velocity components in air

7 $\quad p_{(idx,jdy,kdz)}^{ldt}, v_{x((i+0.5)dx,jdy,kdz)}^{(l+0.5)dt}, v_{y(idx,(j+0.5)dy,kdz)}^{(l+0.5)dt}, v_{z(idx,jdy,(k+0.5)dz)}^{(l+0.5)dt},$ $\qquad$ (12)

8 where dx, dy, and dz are the spatial discretization steps in three directions; dt denotes the

9 time discretization step; and i, j and k are the spatial indices. The acoustic pressure is always

10 updated at times ldt and the velocity components at intermediate times $(l+0.5)dt$.

11 $\quad$ The acoustic pressures p_a and p_f in the porous medium follow the same discretization as

12 the acoustic pressures in air, and the velocity components ($\mathbf{V}_a$ and $\mathbf{V}_f$) in the porous medium

13 follow the same discretization as the particle velocities in air. The parameters ϕ_0, ϕ and Π_n

14 related to leaf vibration are all determined at the same grid positions as the particle velocity

15 components v_{xp} (see Fig. 1), but they are updated at the integer times steps just like the acoustic

16 pressures p:

17 $\quad \phi_{0((i+0.5)dx,jdy,kdz)}^{ldt}, \phi_{((i+0.5)dx,jdy,kdz)}^{ldt}$ and $\Pi_{n((i+0.5)dx,jdy,kdz)}^{ldt}.$ $\qquad$ (13)

18 $\quad$ The discretized forms of Eqs. (1) and (2) read

19 $\quad p_{i,j,k}^{l+1} = p_{i,j,k}^{l} - dt\rho_0 c^2 \sum_{\beta} \dfrac{v_{\beta\,\beta+0.5}^{l+0.5} - v_{\beta\,\beta-0.5}^{l+0.5}}{d\beta},$ $\qquad$ (14)

10

1     $v_{\alpha(\alpha+0.5)}^{l+0.5} = v_{\alpha(\alpha+0.5)}^{l-0.5} - \dfrac{dt}{\rho_0 d\alpha}\left(p_{\alpha+1}^{l} - p_{\alpha}^{l}\right).$ (15)

2   In Eqs. (14) and (15), α represents one of the three Cartesian indices; summation over β

3   runs over all the Cartesian indices; α and β in $\alpha+0.5$, $\alpha+1$ and $\beta\pm0.5$ denote one of

4   the indices i, j and k; v_α and v_β are the velocities in α and β directions, respectively. The

5   pressure at time $(l+1)dt$ is determined by the pressure at previous time ldt and the velocities at

6   time $(l+0.5)dt$. The velocity at time $(l+0.5)dt$ is determined by the velocity at previous time

7     $(l-0.5)dt$ and the pressure at time ldt. Similarly, the discretized forms of the governing equations

8   in the elastic porous media are

9     $p_{ai,j,k}^{l+1} = p_{ai,j,k}^{l} - K_a v_a dt \sum_{\beta} \dfrac{v_{\beta a\,\beta+0.5}^{l+0.5} - v_{\beta a\,\beta-0.5}^{l+0.5}}{d\beta}$

10     $- \left(K_a - P_0\right)v_f dt \sum_{\beta} \dfrac{v_{\beta f\,\beta+0.5}^{l+0.5} - v_{\beta f\,\beta-0.5}^{l+0.5}}{d\beta}$,   (16)

11     $\left(\dfrac{\rho_a m_t}{v_a^{\,2} dt} + \dfrac{\sigma}{2}\right)v_{\alpha a\,i+0.5,j,k}^{l+0.5} = \left(\dfrac{\rho_a m_t}{v_a^{\,2} dt} - \dfrac{\sigma}{2}\right)v_{\alpha a\,i+0.5,j,k}^{l-0.5}$

12     $- \dfrac{p_{ai+1,j,k}^{l} - p_{ai,j,k}^{l}}{d\alpha} + \left(\dfrac{\rho_a\left(m_t/v_a^{\,2} - 1\right)}{dt} + \dfrac{\sigma}{2}\right)v_{\alpha f\,i+0.5,j,k}^{l+0.5}$

13     $- \left(\dfrac{\rho_a\left(m_t/v_a^{\,2} - 1\right)}{dt} - \dfrac{\sigma}{2}\right)v_{\alpha f\,i+0.5,j,k}^{l-0.5}$,   (17)

14     $p_{f\,i,j,k}^{l+1} = p_{f\,i,j,k}^{l} + \dfrac{v_f}{v_a}\left(p_{ai,j,k}^{l+1} - p_{ai,j,k}^{l}\right)$

15     $- dt K_f \sum_{\beta} \dfrac{v_{\beta f\,\beta+0.5}^{l+0.5} - v_{\beta f\,\beta-0.5}^{l+0.5}}{d\beta}$,   (18)

16

$$1 \quad \left(\frac{\rho_f + \rho_a\left(m_t/v_a^2 - 1\right)}{dt} + \frac{\sigma}{2} \right) v_{af\,i+0.5,j,k}^{l+0.5}$$

$$2 \quad = \left(\frac{\rho_f + \rho_a\left(m_t/v_a^2 - 1\right)}{dt} - \frac{\sigma}{2} \right) v_{af\,i+0.5,j,k}^{l-0.5}$$

$$3 \quad - \frac{p_{f\,i+1,j,k}^{l} - p_{f\,i,j,k}^{l}}{d\alpha}$$

$$4 \quad + \left(\frac{\rho_a\left(m_t/v_a^2 - 1\right)}{dt} + \frac{\sigma}{2} \right) v_{\alpha a\,i+0.5,j,k}^{l+0.5}$$

$$5 \quad - \left(\frac{\rho_a\left(m_t - 1\right)}{dt} - \frac{\sigma}{2} \right) v_{\alpha a\,i+0.5,j,k}^{l-0.5} . \qquad (19)$$

6   The discretized form of Eq. (7) for the vibration velocity of the leaf is

$$7 \quad v_{xp\,i+0.5,j,k}^{l+0.5} = \frac{\left(1/dt - R_L/2\right)}{\left(1/dt + R_L/2\right)} v_{xp\,i+0.5,j,k}^{l-0.5} - \frac{1}{\rho_m dx\left(1/dt + R_L/2\right)}\left(p_{i+1,j,k}^{l} - p_{i,j,k}^{l} \right)$$

$$8 \quad - \frac{1}{\rho_m h\left(1/dt + R_L/2\right)} \left(\frac{\phi_{0\,i+0.5,j+1,k}^{l} - 2\phi_{0\,i+0.5,j,k}^{l} + \phi_{0\,i+0.5,j-1,k}^{l}}{dy^2} + \frac{\phi_{0\,i+0.5,j,k+1}^{l} - 2\phi_{0\,i+0.5,j,k}^{l} + \phi_{0\,i+0.5,j,k-1}^{l}}{dz^2} \right)$$

$$9 \quad - \frac{1}{\rho_m h\left(1/dt + R_L/2\right)} \left(\frac{\phi_{i+0.5,j+1,k}^{l} - 2\phi_{i+0.5,j,k}^{l} + \phi_{i+0.5,j-1,k}^{l}}{dy^2} + \frac{\phi_{i+0.5,j,k+1}^{l} - 2\phi_{i+0.5,j,k}^{l} + \phi_{i+0.5,j,k-1}^{l}}{dz^2} \right). \qquad (20)$$

10   In this paper, the thickness of the plate, h, equals the grid size in the direction perpendicular

11   to the plate surface. In Eq. (20), the bending term ϕ_0 is determined by its previous value and the

12   velocity v_{xp} at the intermediate time step

$$13 \quad \phi_{0\,i+0.5,j,k}^{l} = \phi_{0\,i+0.5,j,k}^{l-1}$$

$$14 \quad + Ddt\left(\frac{v_{xp\,i+0.5,j+1,k}^{l-0.5} - 2v_{xp\,i+0.5,j,k}^{l-0.5} + v_{xp\,i+0.5,j-1,k}^{l-0.5}}{dy^2} \right.$$

$$15 \quad \left. + \frac{v_{xp\,i+0.5,j,k+1}^{l-0.5} - 2v_{xp\,i+0.5,j,k}^{l-0.5} + v_{xp\,i+0.5,j,k-1}^{l-0.5}}{dz^2} \right). \qquad (21)$$

1   The damping term ϕ is determined by its value in the previous time step and the velocities

2   v_{xp} from the previous 2 time steps,

3     $\phi_{i+0.5,j,k}^{l} = \phi_{i+0.5,j,k}^{l-1} + dt \sum_{n=1}^{2} DR_n \, \Pi_{ni+0.5,j,k}^{l}$,   (22)

4     $\Pi_{ni+0.5,j,k}^{l} = \Pi_{ni+0.5,j,k}^{l-1} \cdot e^{-s_n dt}$

5     $+ \left(\dfrac{v_{xp\,i+0.5,j+1,k}^{l-0.5} - 2v_{xp\,i+0.5,j,k}^{l-0.5} + v_{xp\,i+0.5,j-1,k}^{l-0.5}}{dy^2} + \dfrac{v_{xp\,i+0.5,j,k+1}^{l-0.5} - 2v_{xp\,i+0.5,j,k}^{l-0.5} + v_{xp\,i+0.5,j,k-1}^{l-0.5}}{dz^2} \right.$

6     $\left. - \dfrac{v_{xp\,i+0.5,j+1,k}^{l-1.5} - 2v_{xp\,i+0.5,j,k}^{l-1.5} + v_{xp\,i+0.5,j-1,k}^{l-1.5}}{dy^2} - \dfrac{v_{xp\,i+0.5,j,k+1}^{l-1.5} - 2v_{xp\,i+0.5,j,k}^{l-1.5} + v_{xp\,i+0.5,j,k-1}^{l-1.5}}{dz^2} \right) \dfrac{1+e^{-s_n dt}}{2}$. (23)

7   The updating equation for the velocity parallel to boundaries, v_γ, is adapted to include the effect

8   of the viscous boundary layer. The square root of ω in Eq. (11) is hereby approximated by a ratio

9   of polynomials of order M and N in frequency domain. Eventually, this leads to the adapted FDTD

10   update equation:

11     $\left(\dfrac{\rho_0}{dt} a_0 + \dfrac{\sqrt{\mu \rho_0}}{2 \cdot d\delta} b_0 \right) v_\gamma^{l+\frac{1}{2}} = -\sum_{k=0}^{M} a_k \dfrac{\partial p^{l-k}}{\partial \gamma}$

12     $- \dfrac{\rho_0}{dt} \sum_{k=1}^{M+1} (a_k - a_{k-1}) v_\gamma^{l-k+\frac{1}{2}} - \dfrac{\sqrt{\mu \rho_0}}{2 \cdot d\delta} \sum_{i=1}^{N+1} (b_i + b_{i-1}) v_\gamma^{l-i+\frac{1}{2}}$,   (24)

13   where $d\delta$ is the grid step in the direction orthogonal to the leaf plane; γ denotes the

14   directions parallel to the leaf surface; and μ is the dynamic viscosity. For the simulations in

15   this paper, M and N are chosen equal to 2. The values for a_k and b_i are the same as those

16   used by Bockstael et al.[21]: $a_0 = 1, a_1 = -1.871, a_2 = 0.87213, a_3 = 0, b_0 = 391.02, b_1 = -769.2,$

17     $b_2 = 378.2$ and $b_3 = 0$. Note that for the special case $a_0 = 1$, and the other coefficients equal to

18   0, Eq. (24) reduces to Eq. (15).

13

1

III. EXPERIMENTAL PROCEDURE

3

4   The effect of a single leaf on the acoustical properties of a porous substrate was investigated

5   with a 29 mm diameter impedance tube in the Acoustics Laboratory at the University of

6   Bradford. In this work the standard material characterization procedure as described in Ref. 22

7   was used to determine the acoustical and related non-acoustical properties of the porous material

8   specimens. Leaves from the following plants were used in this experiment: (i) Japanese

9   Andromeda (*Pieris japonica*: leaf density 0.367 kg/m^2 and thickness 0.41mm); (ii) Scarlet

10   wonder (*Rhododendron forrestii*: leaf density 0.408 kg/m^2 and thickness 0.34mm); (iii) Primrose

11   (*Primula vulgaris*: leaf density 0.469 kg/m^2 and thickness 0.74mm); and (iv) Corsican Hellebore

12   (*Helleborus argutifolius*: leaf density 0.22 kg/m^2 and thickness 0.43mm). A 29mm round cutter

13   was used to cut a specimen from a leaf tissue that could fit accurately the diameter of the

14   impedance tube. These leaf specimens are shown in Fig. 2. Figure 3 illustrates a 25 mm thick

15   sample of Armafoam Sound 240 reconstituted foam supplied by Armacell UK Ltd and a 30 mm

16   thick melamine foam supplied by Foam Techniques Ltd. These materials are well-characterized

17   so that it is possible to use them to represent soil substrates with two contrasting physical

18   properties. Armafoam Sound 240 material has a relatively high density (240 kg/m^3) which does

19   not allow for frame vibration effects in the considered frequency range. This material has a

20   relatively high porosity, $v_a \approx 0.8$, which is akin to that typical for soil substrates used in living

21   wall systems (Khan *et al.*[23]). The flow resistivity of melamine foam is similar to that of porous

1   soil substrate used for the design of living walls. The density of Melamine foam is relatively low

2   (40 kg/m^3) so that the frame vibration cannot be neglected and it is likely to have an effect on the

3   acoustic absorption coefficient of the porous substrate covered by a leaf.

4   Three 1mm diameter nails were inserted in the porous samples to form a support base for the

5   29mm leaf specimen (see Fig. 4). Measurements of the acoustic absorption of Armafoam Sound

6   240 material and Melamine foam with and without nails indicated that the effect of the three

7   nails on the acoustic absorption spectra was negligible and comparable to the reproducibility of

8   the adopted measurement procedure. These nails served as small columns to support the leaf

9   specimen during the measurement and to restrain to some extent the frame vibration when

10   melamine foam was used as a porous substrate. The leaf specimen was placed on the top of the

11   nails in the porous sample in the impedance tube so that there was approximately 1 mm air gap

12   between the leaf and the top surface of the porous sample as illustrated in Fig. 4. In this way

13   there was no mechanical contact between the top surface of the porous sample and the bottom

14   surface of the leaf specimen. Therefore, the leaf was simply supported at three points so that we

15   were able to measure the influence of the leaf vibration and its acoustical shielding effect on the

16   acoustic absorption coefficient of the porous sample that was representing the soil.

17   When the pressure at two microphones in the impedance tube is recorded, the absorption

18   coefficient can be calculated according to ISO10534-2 standard[24]. Firstly, the fast Fourier

19   transform is used to get the frequency spectra of the two pressure signals. Then, these two

20   pressure spectra and the distance between two microphones are used to calculate three

1   parameters, H_I, H_R and H_{12}, which are transfer functions for the incident wave, reflected

2   wave and total sound field, respectively. After that, the reflection coefficient can be calculated by

3    $$r = \frac{H_{12} - H_I}{H_R - H_{12}} e^{2jk_0x_1},$$ (25)

4   where k_0 is wave number and x_1 is the coordinate of the first microphone with reference to

5   the origin, the right end of the impedance tube. Finally, the absorption coefficient can be

6   obtained from

7    $$\alpha_{pm} = 1 - |r|^2.$$ (26)

8   The described measurements were repeated 3 times with the same material specimen. The

9   average was presented as the final results. The reproducibility of the adopted material

10   characterization procedure has been detailed in Ref. 25.

11

12   **IV. NUMERICAL SETUP**

13

14   The settings of 3D numerical simulation are given in this section. Figure 5 shows the cross

15   section of the impedance tube used in the simulation. The diameter of the impedance tube is

16   0.029 m. The porous substrate is placed at the right end of the impedance tube. The distance

17   between the sound source that generates a normal incidence plane wave (at S) and the porous

18   substrate is 0.07 m. The pressure is recorded at two points, M_1 and M_2, which represent the

19   locations of the two microphones in the experimental setup. The first microphone (at point M_1)

20   and the second microphone (at point M_2) are at a distance of 0.03 m and 0.035 m from the source,

1   respectively. A perfectly matched layer (PML)[26] is used at the left end of the impedance tube as

2   a non-reflecting boundary condition.

3   For all the simulations in this paper, the spatial discretization step is 0.001 m in all three

4   coordinate directions, and the time step dt equals 1.6981×10^{-6} s, yielding a Courant number of 1.

5   To generate the normal incidence plane wave, a Gaussian modulated pulse is added to all grid

6   points lying in the source plane:

7     $$S = A_S \sin(2\pi f_c t)\exp\left[-a(t-t_c)^2\right], \tag{27}$$

8   where A_S is amplitude of the source, f_c is central frequency, t_c is central time, and a is

9   the parameter determining the signal bandwidth. The following values are chosen: $f_c = 3000\,\text{Hz}$,

10     $t_c = 5dt$, and $a = 1.6 \times 10^7$. The value of A_S has no meaning, since spectral division has been

11   applied during post-processing of the time-domain responses. It is guaranteed that all sound

12   frequencies of interest are sufficiently excited, and that a smooth course of the pulse over time is

13   obtained.

14   For the numerical simulation in the poro-elastic substrate, it is assumed that the adiabatic

15   index equals 1.4 and the ambient pressure (P_0) is 0.1 MPa. The mass of air per unit volume (ρ_0)

16   is 1.2 kg/m^3. Other material parameters are slightly tuned as explained in Sec. V.

17   The pressure spectra at the two points (M$_1$ and M$_2$ in Fig. 5) are obtained by using a fast

18   Fourier transform on the time-domain signals. Then, the absorption coefficient can be calculated

19   according to Eqs. (25) and (26).

20

V. COMPARISON WITH EXPERIMENTAL RESULTS

In this section, the absorption coefficient for the porous substrate with and without leaf is calculated. The results of these calculations are compared against the data obtained from the impedance tube measurements. Firstly, the leaf effect is not considered and the physical parameters of the porous substrate are determined. These parameters are porosity, flow resistivity, tortuosity, bulk modulus, and damping coefficient of the material frame. Secondly, the effect of a leaf on the absorption of the porous substrate is studied. In this step, the influences of the bending stiffness of the leaf and the leaf surface density have to be determined as well.

A. Porous substrate without foliage

A trial-and-error approach has been applied in order to obtain a good fit between measurements and simulations. Initial values are the measured quantities and parameters for similar materials as found in literature.

Figure 6 shows the absorption coefficient spectrum of a 25 mm thick Armafoam Sound 240 specimen, whose density is 240kg/m^3, in the presence of a hard termination. A good fit between measurements and predictions is obtained when choosing the following material parameters: the porosity (v_a) equal to 0.81; tortuosity (m_t) equal to 8.4; flow resistivity (σ) equal to 260 kPa·s·m^{-2}; the bulk modulus of the substrate material (K_f) equal to 0.67 MPa and a damping coefficient (R_f) for the frame of 1600 kPa·s·m^{-2}. The fitted porosity, tortuosity and flow resistivity are compared with the non-acoustic measured results using the standard material

18

1   characterization procedure; and the comparison is given in Table I. From this comparison and the

2   results in Fig. 6, it can be concluded that the implemented FDTD equations can give a good and

3   realistic prediction of the absorption coefficient of this type of porous substrate.

4   Figure 7 shows the absorption coefficient of 30mm thick melamine foam, having a much

5   smaller density, 40kg/m^3. For this substrate, the one-fourth wavelength frame resonance[27] occurs

6   around 2700 Hz. At this frequency, the wavelength is around 4 times of the thickness of the

7   melamine foam. The numerical model is able to simulate this frame resonance and predict

8   accurately the absorption coefficient of Melamine foam across the considered frequency range.

9   The following values of the five non-acoustical parameters provide the best fit between the

10 acoustic model and measured data: the porosity (v_a) equal to 0.98; tortuosity (m_t) equal to 1.22;

11 flow resistivity (σ) equal to 22 kPa·s·m^{-2}; the bulk modulus of the substrate material (K_f) equal

12 to 1.24 MPa and the damping coefficient (R_f) equal to 20 kPa·s·m^{-2}. The comparison of the

13 fitted porosity, tortuosity and flow resistivity for this melamine foam with the measured values

14 published by Dragonetti et al.[28] and Kino and Ueno[29] is given in Table II. It is shown that these

15 fitted parameters for the melamine foam are realistic.

16

17 **B. Porous substrate with foliage**

18   In this section, a single leaf, which fully covers the cross section of the impedance tube, is

19 placed in front of the porous substrate and the distance between the leaf and the substrate is set to

20 1 mm. The four leaves described in Sec. III were considered. The bending stiffness of each leaf

21 was estimated according to the following expression[15]

19

1 $$D = \frac{E \cdot h^3}{12(1-v^2)},$$ (28)

2 where E is the Young's modulus and v is the Poisson's ratio. Equation (28) has previously

3 been used to determine the bending stiffness in a thin uniform homogeneous plate[15].

4 For the leaves used in this paper, the average thickness has been given in Sec. III. Earlier

5 work suggests that the Poisson's ratio of an isotropic leaf specimen is close to 0.25[30]. For the

6 leaf's Young's modulus, the work done by T. Saito et al.[31] and U. Niinemets[32] can be used as a

7 first estimate. T. Saito et al.[31] presented a linear regression relationship between bulk elastic

8 modulus (ε) and Young's modulus (E) for the leaves of *Quercus glauca* and *Quercus serrata*:

9 $\varepsilon = AE + B$. (29)

10 For *Quercus glauca*, $A = 0.11$ and $B = 1.21$ result in a regression with $r_{cc}^2 = 0.78$, where r_{cc}

11 is the correlation coefficient; for *Quercus serrata*, $A = 0.13$ and $B = -1.42$ give $r_{cc}^2 = 0.84$.

12 Niinemets[32] presented a linear regression relationship between leaf volume density and its bulk

13 modulus based on the data from 51 tree and shrub species:

14 $\varepsilon = 2.03 + 25.4\rho_L$, with $r_{cc}^2 = 0.35$, (30)

15 where ε is the foliage bulk elastic modulus and ρ_L is the leaf volume density. The leaf

16 volume density for Japanese Andromeda, Scarlet wonder, Primrose and Corsican Hellebore can

17 be calculated according to the data given in Sec. III, yielding 895kg/m^3, 1200kg/m^3, 634kg/m^3

18 and 512kg/m^3, respectively. According to Eq. (30), the bulk elastic modulus for Japanese

19 Andromeda, Scarlet wonder, Primrose and Corsican Hellebore can be estimated to be 24.8 MPa,

20 32.5 MPa, 18.1 MPa and 15 MPa, respectively. Then, these values can be used in Eq. (29) to get

the estimations for the leaves' Young's modulus. Finally, the bending stiffness can be calculated

using Eq. (28). This finally gives as a rough estimate for bending stiffness equal to 0.0025 N·m,

0.0018 N·m, 0.01 N·m and 0.0017 N·m for each of the four leaves.

The absorption coefficients for the 25 mm Armafoam Sound 240 foam with three different

leaves (Japanese Andromeda, Scarlet wonder and Primrose) are shown in Figs. 8 - 10. The

simulation results in Figs. 8(a), 9(a) and 10(a) don't consider the influence of the leaf bending

stiffness; and they are smoother, when compared to the measurements. While, in Figs. 8(b), 9(b)

and 10(b), the effect of the bending stiffness on the predicted absorption coefficient of the porous

substrate covered by a leaf is included in the simulation results. It can be found that when

bending stiffness is considered, the absorption coefficient follows the same trend as that without

considering leaf bending, but obvious fluctuations can be noticed, which show qualitatively

agreement with the measurements. The bending stiffness given in Figs. 9 and 10 is modified

from the theoretical estimates discussed above to improve correspondence with measurements. A

possible reason for this difference is that Eq. (29) is based on the leave from *Quercus glauca* and

Quercus serrata, which both have a relative flat surface. In contrast, the leaves from Scarlet

wonder and Primrose have a rather uneven surface (see Fig. 2). As a result Eq. (29) becomes less

accurate and also makes it more difficult to obtain the correct leaf thickness, which has a strong

effect on density and an even stronger effect on bending stiffness (third power dependency

according to Eq. (28)). For the leaf from Japanese Andromeda, using the calculated bending

stiffness gives absorption coefficient that fits the measurements better because this kind of leaf

has a flat surface.

Figure 11 shows the absorption coefficient for the 30 mm melamine foam with Corsican

Hellebore leaf. Unlike Figs. 8 - 10, Fig. 11 does not show results including leaf bending as no

effect of the latter was observed. A possible reason for this phenomenon is that the rather large

absorption coefficient of the 30mm melamine foam generates much weaker standing waves

between leaf and porous foam. As a result, the leaf bending does not influence the overall

absorption characteristics significantly.

The results presented in Figs. 8 - 11 show that in the presence of a leaf the absorption

coefficient of a porous substrate decreases in the high frequency range beyond 2000-3000 Hz,

increases in the middle frequency range between 500 Hz and 2000 Hz and keeps unaffected in

the low frequency range below 250 Hz. Although the agreement between measurements and

simulations is generally close, there are some discrepancies. These can be attributed to the

complex structure of the leaf, which is simplified in the numerical predictions. For example, the

extension of the veins of leaf and the uneven distribution of the leaf surface density could give

rise to deviations from the assumed uniform properties of the leaf. It is also difficult to ensure

that there is no circumferential gap between the edge of the leaf and the wall of the impedance

tube and that the mechanical boundary conditions on the edge of the leaf are accurately modeled.

C. The influence of leaf surface density

In this section, the effect of leaf surface density is numerically studied and the bending

stiffness is set to 0. The leaf surface density is a parameter that is likely to vary largely from plant

to plant. On the other hand, this is a parameter that is rather easy to quantify and use in the model

22

1   so that the predicted results can be directly translated into practical applications. The effect of the

2   leaf surface density on the absorption coefficient of the AFS240 foam and Melamine foam

3   samples was modeled here and the results are shown in Figs. 12 - 13, respectively.

4   The results presented in these figures suggest that below 1-2 kHz the effect of leaf surface

5   density on the combined leaf-foam absorption system is relatively small and that above 1-2 kHz

6   this effect becomes more pronounced. The absorption coefficient of the porous substrate covered

7   by a leaf increases with the decreased leaf surface density. Furthermore, the presence of a leaf

8   with a lower surface density results in absorption coefficient enhancement across a wider

9   frequency range than in the case of a leaf with a higher surface density. This effect is particularly

10   obvious for the low-permeability AFS240 foam. Specifically, Fig. 12 shows that adding a leaf

11   with the surface density of 100 g/m^2 can increase the absorption coefficient up to 20% below

12   4000 Hz, while adding a leaf with a larger surface density results in absorption enhancement

13   limited to frequencies below 2500 Hz. For the high-permeability foam, changes in absorption

14   coefficient by adding a leaf are even stronger. The decrease in absorption at higher frequencies is

15   more pronounced for leaves with a higher surface density.

16   Two conclusions can be drawn from these results: (i) introducing a low-density leaf to the

17   vicinity of a porous surface results in the enhancement in the low frequency absorption

18   coefficient; (ii) this effect is particularly pronounced in the case of a low-permeability porous

19   substrate; (iii) at high frequencies, there is a decrease in absorption.

20

VI. CONCLUSIONS

The influence of loose leaves on the acoustic absorption of a porous substrate for normal incident wave is studied experimentally and numerically. The equations based on the Biot's elastic frame porous medium model and isotropic plate vibration theory are solved using a finite-difference time-domain approach. This approach enables accurate prediction for the absorption coefficient spectrum of a leaf in front of the surface of a porous substrate. The predictions were made using non-acoustical parameters which were deduced from the absorption coefficient spectra of porous specimens measured at normal incidence in the absence of leaf. The changes in the absorption coefficient spectra caused by the leaf vibration were closely predicted. Both the experimental data and numerical model predictions show that the absorption characteristics change noticeably when a leaf is added to the porous substrate. Typically, an unaffected change in the absorption coefficient spectrum in low frequency range (below 250 Hz), an increase in the middle frequency range (500 Hz-2000 Hz) and a decrease in the higher frequency range (beyond 2000-3000 Hz) are observed. The influence of the leaf becomes more pronounced when the leaf is added to the low-permeability substrate. The increase in absorption coefficient by leaves is in the typical frequency range of road traffic noise, while the negative effect by the presence of leafs is observed at sound frequencies that are typically too high to be of importance in environmental acoustics.

6

7 **REFERENCES**

[1]W. Huisman and K. Attenborough, "Reverberation and Attenuation in a Pine Forest," J. Acoust. Soc. Am. **90**, 2664–2677 (1991).

[2]K. Attenborough, K. M. Li and K. Horoshenkov, *Predicting Outdoor Sound* (Taylor & Francis, New York, 2007), pp. 311–321.

[3]K.V. Horoshenkov, A. Khan, H. Benkreira and A. Mandon, "The effect of moisture and soil type on the acoustical properties of green noise control elements," Proceedings of Forum Acusticum 2011, Aalborg, Denmark, 845–849 (2011).

[4]N. H. Wong, A. Y. K. Tan, P. Y. Tan, K. Chiang and N. C. Wong, "Acoustics evaluation of vertical greenery systems for building walls," Build. Environ. **45**, 411–420 (2010).

[5]T. Van Renterghem, E. Salomons and D. Botteldooren, "Parameter study of sound propagation between city canyons with a coupled FDTD-PE model," Appl. Acoust. **67**, 487–510 (2006).

[6]M. Hornikx and J. Forssén, "Noise abatement schemes for shielded canyons," Appl. Acoust. **70**, 267–283 (2009).

[7]T. Van Renterghem and D. Botteldooren, "In-situ measurements of sound propagating over extensive green roofs," Build. Environ. **46**, 729–738 (2011).

[8]T. Van Renterghem and D. Botteldooren, "Reducing the acoustical façade load from road traffic with green roofs," Build. Environ. **44**, 1081–1087 (2009).

[9]T. Van Renterghem and D. Botteldooren, "Numerical evaluation of sound propagating over green roofs," J. Sound Vibr. **317**, 781–799 (2008).

[10]E. M. Salomons, R. Blumrich and D. Heimann, "Eulerian time-domain model for sound propagation over a finite-impedance ground surface. Comparison with frequency-domain models," Acta Acust. United Acust. **88**, 483–492 (2002).

[11]K. Attenborough, I. Bashir and S. Taherzadeh, "Outdoor ground impedance models," J. Acoust. Soc. Am. **129**, 2806–2819 (2011).

[12]K. Wilson, V. Ostashev, S. Collier, N. Symons, D. Aldridge and D. Marlin, "Time-domain calculations of sound interactions with outdoor ground surfaces," Appl. Acoust. **68**, 173–200 (2007).

[13]M. A. Biot, "Theory of Propagation of Elastic Waves in a Fluid-Saturated Porous Solid. I. Low-Frequency Range," J. Acoust. Soc. Am. **28**, 168–178 (1956).

[14]M. A. Biot, "Theory of Propagation of Elastic Waves in a Fluid-Saturated Porous Solid. II. High-Frequency Range," J. Acoust. Soc. Am. **28**, 179–191 (1956).

[15]F. Fahy, *Foundation of Engineering Acoustics* (Academic Press, London, 2001), pp. 285–287.

[16]A. Chaigne and C. Lambourg, "Time-domain simulation of damped impacted plate. I. Theory

and experiments," J. Acoust. Soc. Am. **109**, 1422–1432 (2001).

[17]C. Lambourg, A. Chaigne and D. Matignon, "Time-domain simulation of damped impacted plate. II. Numerical model and results," J. Acoust. Soc. Am. **109**, 1433–1447 (2001).

[18]M. J. M. Martens and A. Michelson, "Absorption of acoustic energy by plant leaves," J. Acoust. Soc. Am. **69**, 303-306 (1981).

[19]D. Botteldooren, "Vorticity and entropy boundary conditions for acoustical finite-difference time-domain simulations," J. Acoust. Soc. Am. **102**, 170-178 (1997).

[20]D. Botteldooren, "Acoustical finite-difference time-domain simulation in a quasi-Cartesian grid," J. Acoust. Soc. Am. **95**, 2313–2319 (1994).

[21]A. Bockstael, B. de Greve, T. Van Renterghem, D. Botteldooren, W. D'Haenens, H. Keppler, L. Maes, B. Philips, F. Swinnen and B. Vinck, "Verifying the attenuation of earplugs in situ: Method validation using artificial head and numerical simulations," J. Acoust. Soc. Am. **124**, 973-981 (2008).

[22]S. Mahasaranon, K. V. Horoshenkov, A. Khan, H. Benkreira, "The effect of continuous pore stratification on the acoustic absorption in open cell foams," J. Appl. Phys. **111**, 084901 (2012).

[23]K. V. Horoshenkov, A. Khan, H. Benkreira, A. Mandon and R. Rohr, "The effect of moisture and soil type on the acoustical properties of green noise control elements," Proceedings of Forum Acusticum 2011, Aalborg, Denmark, (2011).

[24]ISO 10534-2, "Acoustics-Determination of sound absorption coefficient and impedance in impedance tubes-Part 2: Transfer-function method," International Organization for

Standardization (Geneva, Switzerland, 1998).

[25]K. V. Horoshenkov, A. Khan, F.-X. Bécot, L. Jaouen, F. Sgard, A. Renault, N. Amirouche, F. Pompoli, N. Prodi, P. Bonfiglio, G. Pispola, F. Asdrubali, J. Hübelt, N. Atalla, C. K. Amédin, W. Lauriks, L. Boeckx, "Reproducibility experiments on measuring acoustical properties of rigid-frame porous media (round-robin test)," J. Acoust. Soc. Am. **122**, 345-353 (2007).

[26]J. P. Berenger, "A perfectly matched layer for the absorption of electromagnetic waves," J. Comput. Phys. **114**, 185–200 (1994).

[27]J. Allard and N. Atalla, Propagation of Sound in Porous Media: Modelling Sound Absorbing Materials (John Wiley & Sons Ltd, UK, 2009), pp. 129-130.

[28]R. Dragonetti, C. Ianniello and R. A. Romano, "Measurement of the resistivity of porous materials with an alternating air-flow method," J. Acoust. Soc. Am. **129**, 753-764 (2008).

[29]N. Kino and T. Ueno, "Comparisons between characteristic lengths and fibre equivalent diameters in glass fibre and melamine foam materials of similar flow resistivity," Appl. Acoust. 69, 325–331 (2008).

[30]K. J. Niklas, *Plant Biomechanics: An Engineering Approach to Plant form and Function* (The University of Chicago Press, Chicago, 1992), pp. 68–72.

[31]T. Saito, K. Soga, T. Hoson and I. Terashima, "The bulk elastic modulus and the reversible properties of cell walls in developing *Quercus* leaves," Plant Cell Physiol. **47**, 715–725 (2006).

[32]U. Niinemets, "Global-scale climatic controls of leaf dry mass per area, density, and thickness in trees and shrubs," Ecology **82**, 453–469 (2001).

1

1　**List of Tables**

2　Table I. Comparison between the fitted porosity (v_a), tortuosity (m_t) and flow resistivity (σ:

3　KPa·m·s^{-2}) of the Armafoam Sound 240 foam and the non-acoustic measured results using the

4　standard material characterization procedure (Ref. 22).

	Fitted values	Measured value
v_a	0.81	0.812
m_t	8.4	7.37
σ	260	254

5

1 Table II. Comparison between the fitted porosity (v_a), tortuosity (m_t) and flow resistivity (σ:

2 KPa·m·s^{-2}) of the melamine foam with the published measured results by Dragonetti et al.(Ref.

3 28) and Kina and Ueno (Ref. 29).

	Fitted values	Dragonetti et al.	Kino and Ueno
v_a	0.98	0.93	0.992-0.995
m_t	1.22	1.05	1.0053-1.0059
σ	22	10.7	10.5-17.5

4

List of Figures

FIG. 1. Spatial organization of the staggered grids for different materials. The left grid denotes the cell in air. The middle grid denotes the cell including the leaf. The star symbol on the right cell-plane which is perpendicular to x-axis denotes the site for the parameters ϕ_0, ϕ and Π_n. The right grid denotes the cell in the porous media. There are two pressures and two groups of velocity components shown in this grid, for air and solid frame, respectively. The double arrow denotes the velocity components for the solid frame.

FIG. 2. Photographs of the leaves used in the acoustic experiment. (Color online)

FIG. 3. Photographs of the porous material samples used in the acoustic experiments, (a) Armafoam Sound 240, (b) Melamine foam.

FIG. 4. The arrangement for the leaf support over the porous substrate: (a) dimensions of leaf support, the distance between two supports is 15 mm and the distance from support to the foam edge is 5.5 mm; (b) leaf on top of melamine foam.

FIG. 5. Cross section of the impedance tube used in the numerical simulation. A plane wave sound source is located at S. Points M_1 and M_2 indicate the locations of two microphones. The leaf is placed at L, and the gap between leaf and porous substrate is 0.001 m. (Color online)

1   FIG. 6. The absorption coefficient for a 25 mm hard-backed layer of Armafoam Sound 240 foam.

2

3   FIG. 7. The absorption coefficient for a 30 mm hard-backed layer of Melamine foam.

4

5   FIG. 8. The absorption coefficient of a 25 mm hard-backed layer of Armafoam Sound 240 foam

6   covered with a Japanese Andromeda leaf: (a) $D=0$; (b) $D=0.0025$ N·m.

7

8   FIG. 9. The absorption coefficient of a 25 mm hard-backed layer of Armafoam Sound 240 foam

9   covered with a Scarlet wonder leaf: (a) $D=0$; (b) $D=0.004$ N·m.

10

11   FIG. 10. The absorption coefficient of a 25 mm hard-backed layer of Armafoam Sound 240 foam

12   covered with a primrose leaf: (a) D=0; (b) D=0.002 N·m.
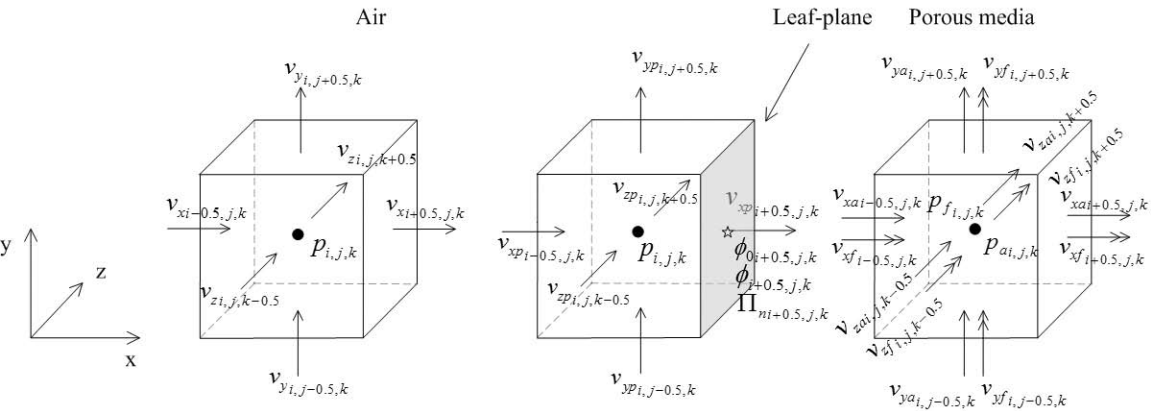
13

14   FIG. 11. The absorption coefficient of a 30 mm hard-backed layer of Melamine foam covered

15   with Corsican Hellebore leaf.

16

17   FIG. 12. The effect of leaf surface density on the absorption coefficient of a 25mm hard-backed

18   layer of Armafoam Sound 240.

19

20   FIG. 13. The effect of leaf surface density on the absorption coefficient of a 30mm hard-backed

21   Melamine foam.

32

(a) Pieris Japonica   (b) Scarlet Wonder

(c) Primrose   (d) Argutifolius

(a)   (b)

(a)   (b)

PML M_1 M_2 Porous substrate

S   L

(a)

(a)

(a)

Legend:
- Simulation: Primrose
- Measurement: Primrose
- Simulation: No Leaf

Absorption coefficient vs Frequency (Hz)

The chart shows Absorption coefficient (y-axis, 0 to 1) versus Frequency (Hz) (x-axis, 0 to 7000), with three curves:
- Simulation: Argutifolius
- Measurement: Argutifolius
- Simulation: No Leaf

Figure showing Absorption coefficient versus Frequency (Hz). Legend: SD=100g/m², SD=300g/m², SD=500g/m², SD=700g/m², SD=900g/m², No Leaf.

Absorption coefficient vs. Frequency (Hz)

Legend:
- SD=100g/m² (∗)
- SD=300g/m² (○)
- SD=500g/m² (dash-dot)
- SD=700g/m² (dashed)
- SD=900g/m² (dotted)
- No Leaf (solid)